Desalination and Water Treatment
www.deswater.com

doi: 10.1080/19443994.2015.1110840

57 (2016) 20377–20387
September

Taylor & Francis
Taylor & Francis Group

Cr(VI) adsorption from aqueous solutions onto Mg–Zn–Al LDH and its corresponding oxide

Gh. Eshaq[a,*], A.M. Rabie[a], A.A. Bakr[b], A.H. Mady[a], A.E. ElMetwally[a]

[a]*Department of Petrochemicals, Egyptian Petroleum Research Institute, Nasr City, Cairo 11727, Egypt, Tel. +201 228289661; email: ghadaamer2002@yahoo.com (G. Eshaq), Tel. +201 227135228; email: abdo3040@yahoo.com (A.M. Rabie), Tel. +201 115025588; emails: amr_mady@yahoo.com (A.H. mady), ahmed_ezzatt@msn.com (A.E. ElMetwally)*
[b]*Department of Analysis and Evaluation, Egyptian Petroleum Research Institute, Nasr City, Cairo 11727, Egypt, Tel. +201 221004221; email: als_water@yahoo.com*

Received 8 April 2015; Accepted 6 October 2015

ABSTRACT

Mg–Zn–Al LDH and its corresponding oxide were successfully employed for Cr(VI) removal from aqueous solutions. Maximum adsorption capacity of 29.25 and 33.82 mg g^{-1} for Mg–Zn–Al LDH and calcined Mg–Zn–Al LDH, respectively, was achieved using Cr(VI) initial concentration of 70 mg L^{-1}, 0.2 g L^{-1} of adsorbent, stirring rate of 160 rpm, pH 6, a contact time of 105 min, and a reaction temperature of 298 K. The results show that the adsorption of Cr(VI) through the rehydration of calcined Mg–Zn–Al LDH is considerably higher than that through the anion exchange of Mg–Zn–Al LDH. Cr(VI) removal from aqueous solutions takes place via either anion exchange between interlayer anions of LDHs and Cr(VI) oxyanions or surface complexation between Cr(VI) oxyanions and inner and outer hydroxyl groups of LDH surfaces.

Keywords: Layered double hydroxide; Cr(VI); Adsorption; Wastewater treatment

1. Introduction

The removal of toxic heavy metals from environmental water resources introduced by industrial pollution is considered a global environmental issue. Chromium is one of the heavy metals and its compounds are extensively used in chemical industries such as electroplating, textile, leather tanning, metal finishing, wood preservation, electroplating, and chromate preparation industries [1,2]. Unlike other common heavy metals such as lead or cadmium, chromium primarily exists in the form of anion Cr(VI) and cation Cr(III) in aqueous environment [3]. Cr(VI) presents the highest environmental threat in aqueous systems, due to its toxicity to biological organisms, high solubility, and mobility. The toxicological effects of Cr(VI) originate on its oxidative nature in water, as well on the formation of free radicals during the reduction of Cr(VI) to Cr(III) occurring inside the cell [4]. Consequently, the World Health Organization recommends a 0.05 mg L^{-1} maximum contaminant level of Cr(VI) in drinking water, [5] while total chromium should be discharged below 2 mg L^{-1} according to US EPA regulations [6].

During recent years, various treatment processes have been employed to remove Cr(VI) from water, for example, chemical treatment, ion exchange, reverse osmosis, electrochemical reduction, and membrane

*Corresponding author.

separation [7]. Most of these methods suffer from drawbacks like high capital and operational cost and problems in disposal of the residual metal sludges [8]. Among these methods, adsorption is extensively used because of the feasibility and low cost. To minimize processing costs, several investigations have focused on the use of low-cost adsorbents, such as chitosan [9–11], waste materials [12], activated carbon [13], coal [14], and polymers [15,16]. However, most of these adsorbents have some flaws, for instance, excessive time requirements, high costs, and inefficiency. Therefore, it is urgent to explore a highly efficient adsorbent.

Layered double hydroxides (LDHs), also known as hydrotalcite-like compounds, are a class of naturally occurring anionic clays. Their basic structure resembles that of brucite, $Mg(OH)_2$, in which a fraction x of divalent cations is isomorphously replaced by trivalent cations, rendering positively charged layers. The charge is electrically balanced by anionic species located in interlayer galleries, along with hydration water molecules. Given the variety of compounds with LDH structure that may be prepared, they are represented by the general formula: $[M^{2+}_{(1-x)}\,M^{3+}_{x}(OH)_2]A^{n-}_{x/n}\cdot]\ mH_2O$. The divalent and trivalent cations are mainly those from the third and fourth periods of the periodic classification of the elements, i.e. those with ionic radii similar to Mg^{2+} and that are capable of occupying the octahedral interstices of the brucite-like lattice. It is also possible to introduce three or even four metal cations in the layers, and to prepare LDHs with M^{+}-M^{3+} or M^{2+}-M^{4+} combinations [17,18]. Meanwhile, the charge-balancing anions A^{n-} are typically carbonates or halogens, although nearly any organic or inorganic anion may be intercalated [19,20]. Upon calcination, the structure progressively loses physisorbed and interlayer water molecules, layer OH groups, and charge-balancing anions, and finally, the layered structure collapses and a mixed oxide solid is formed. This mixed oxide typically presents large specific surface areas, thermal stability, and synergic interactions between the different metal components. Therefore, LDH calcination products have found numerous applications in various catalytic processes [21–23].

Owing to the features of high structural positive charge density, large surface area, high anion exchange capacity, and flexible interlayer space, LDHs exhibit excellent ability to capture organic and inorganic anions. A lot of work has been carried out on the use of LDHs and their calcined products (LDOs) in the removal of various water contaminants [24–27]. Lazaridis and Asouhidou [28] studied the sorptive removal of Cr(VI) from aqueous solutions by calcined Mg–Al–CO_3 hydrotalcite, which presented a sorption capacity of approximately 120 mg Cr/g. Alvarezayuso and Nugteren [29] reported the use of calcined and uncalcined Mg–Al–CO_3-hydrotalcite in the purification of Cr(VI) finishing wastewaters with a maximum removal capacity of 16.3 mg Cr/g on uncalcined hydrotalcite and 128 mg Cr/g on calcined hydrotalcite. Recently, Yu et al. [30] reported that 3D hierarchical flower-like calcined Mg–Al LDHs showed excellent performance in the removal of Cr(VI) from aqueous solutions. Xiao et al. [31] studied the influence of ferric iron in calcined nano-Mg/Al hydrotalcite on the removal of Cr(VI) from aqueous solution; however, the thermodynamic studies revealed that the addition of Fe^{3+} was disadvantageous to adsorption process. Kameda et al. [32] studied the removal of Cr (VI) from aqueous solution using Mg–Al LDHs (Mg–Al LDH) doped with Fe^{2+}. However, we have found no reports on the use of Mg–Zn–Al LDHs and its corresponding oxide in the removal of Cr(VI) from wastewater.

In this study, Mg–Zn–Al LDH and its corresponding oxide were prepared and tested in the removal of Cr(VI) from aqueous solution. The effects of contact time, solution pH, initial concentrations, and adsorbent mass on the removal of Cr(VI) were investigated.

2. Experimental

2.1. Materials

$Al(NO_3)_3{\cdot}9H_2O$, K_2CO_3, and KOH were obtained from Sigma-Aldrich. $Mg(NO_3)_2{\cdot}6H_2O$, $K_2Cr_2O_7$, and $Zn(NO_3)_2{\cdot}6H_2O$ were purchased from Loba Chemie Co.

2.2. Catalyst preparation

The LDHs containing Mg–Zn–Al were synthesized by co-precipitation at low super saturation conditions and at constant pH [33]. A salt solution (1,097.7 mL) was first prepared containing 182.5 g of $Mg(NO_3)_2{\cdot}6H_2O$, 68.13 g of $Zn(NO_3)_2{\cdot}6H_2O$, and 117.7 g of $Al(NO_3)_3{\cdot}9H_2O$. This salt solution was then added to an alkaline solution (100 mL) containing 2 M of K_2CO_3 and KOH, at a controlled pH of 9. The precipitate obtained was kept under vigorous mechanical stirring, at a temperature of 80 ℃ for 18 h. Afterward, the product was thoroughly washed with hot deionized water in order to eliminate excess ions and dried at 100 ℃ for 24 h. The M^{II}/M^{III} molar ratio was kept constant at 2. The obtained sample was calcined at 450 ℃ for 5 h prior to adsorption.

2.3. Characterization

Fourier transform infrared spectroscopy (FTIR) measurements were performed using a Nicolet IS-10 FTIR instrument with KBr disks. X-ray diffraction (XRD) patterns of the samples were recorded in the range $2\theta = 4^\circ$–80° using a Philips powder diffractometer with Cu Kα radiation ($k = 0.154$ nm). The instrument was operated at 40 kV and 40 mA. The spectra were recorded with a 2θ step of 0.02° at a scanning rate of 2° θ/min. Elemental analysis of Mg–Zn–Al LDH was performed using X-ray fluorescence (XRF) instrument with channel control model Pw1390 (Philips) and spectrometer model Pw 1410. Surface area, pore volume, and average pore size were obtained from the N_2 adsorption–desorption isotherms determined at −196°C using a Quantachrome Nova 3200 instrument (USA). Prior to measurements, the samples were perfectly degassed at 100°C for 12 h under vacuum (10–5 mm Hg). Thermogravimetric analysis (TGA) was carried out using the differential thermal analyzer DTA-7, Perkin-Elmer apparatus.

2.4. Adsorption method

Solutions of Cr(VI) with various concentrations (10–90 mg L^{-1}) were freshly prepared by dissolving $K_2Cr_2O_7$ in deionized water. The pH values of the solutions were adjusted using standard acid (0.01 M HNO_3) and base solutions (0.125 M NaOH). The pH of the solution was measured using a pH meter (Thermo Orion 5 Star) equipped with a combined glass electrode (Orion 81–75). The pH meter was calibrated with buffers of pH 4.0 and 7.0 prior to any measurement. Adsorption experiments were carried out with a certain amount of the adsorbents and 100 mL of Cr(VI) solution in a conical flask at 298 K. The effect of adsorbent concentration was tested in the range of 0.1–0.4 g L^{-1}. The effect of contact time was studied in the time range of 15–135 min, and the effect of pH was investigated in the range of 2.0–10.0. Under constant stirring (160 rpm), the reaction solution was extracted at different time intervals and then centrifuged at 3,000 rpm for 15 min. Cr(VI) concentration was determined using Spectrophotometer, LaMotte, model SMART Spectro, USA, and the obtained solids was analyzed.

The amount of adsorption q_e (mg g^{-1}) and the percentage of removal were calculated by the following equations [27,34]:

$$q_e = \frac{V(C_o - C_e)}{m} \quad (1)$$

$$\text{Adsorption}\,(\%) = \frac{(C_o - C_e)}{C_o} \times 100 \quad (2)$$

where C_o and C_e are the initial Cr(VI) concentration and the concentration at equilibrium in mg L^{-1}, m is the mass of the adsorbent and V is the volume of solution.

3. Results and discussion

3.1. Characteristics of the prepared samples

The XRD patterns of the prepared samples are shown in Fig. 1. The XRD pattern of Mg–Zn–Al LDH reveals that the most intense peaks are located at lower 2θ while the least intense peaks are at higher 2θ values. It is obvious that the XRD pattern of Mg–Zn–Al LDH exhibits the Bragg reflections of basal planes as shown in Fig. 1. The sharp and symmetric peaks at the basal (0 0 3), (0 0 6), and (1 1 0) reflections around 2θ ~11°, 2θ ~ 22.8°, and 2θ ~ 60°, respectively, correspond to the basal and in-plane spacing, which are characteristic for the brucite-like layer with a high degree of crystallinity. In addition, the d003 spacing was found to be 7.8 Å, which is within the accepted range for a LDH structure. The XRD pattern of Mg–Zn–Al after Cr(VI) adsorption shows that the features at (0 0 3), (0 0 6), and (1 1 0) are essentially maintained after Cr(VI) adsorption. This indicates that the adsorption of Cr(VI) on Mg–Zn–Al LDH is a surface adsorption phenomenon via surface complexation through the chemical and physical complex between Cr(VI) anions and protonated hydroxyl groups of the LDH surfaces. Compared with pristine Mg–Zn–Al LDH, the (0 0 3) reflection pattern of Mg–Zn–Al LDH after adsorption is slightly shifted to a lower angle, indicating that the d-spacing increased. This indicates that Cr(VI) anions were intercalated into the LDH via anion exchange.

The XRD pattern of the calcined Mg–Zn–Al LDH (Fig. 1) shows that the structure of Mg–Zn–Al LDH is altered upon calcination at 450°C for 5 h. After calcination, the (0 0 3) and (0 0 6) reflections disappear, indicating that the Mg–Zn–Al LDH structure is destroyed and the stacking of the layers becomes disordered. Only few diffused peaks at 35° and 40° are observed, which are attributed to MgO. The reappearance of the characteristic layered structure of Mg–Zn–Al LDH at (0 0 3), (0 0 6), and (1 1 0) after Cr(VI) adsorption is an indication for the "memory effect" of the Mg–Zn–Al LDH.

Unit cell parameters c and a, listed in Table 1, are obtained by Bragg's law. The unit cell parameter a is related to the cation–cation distance within the

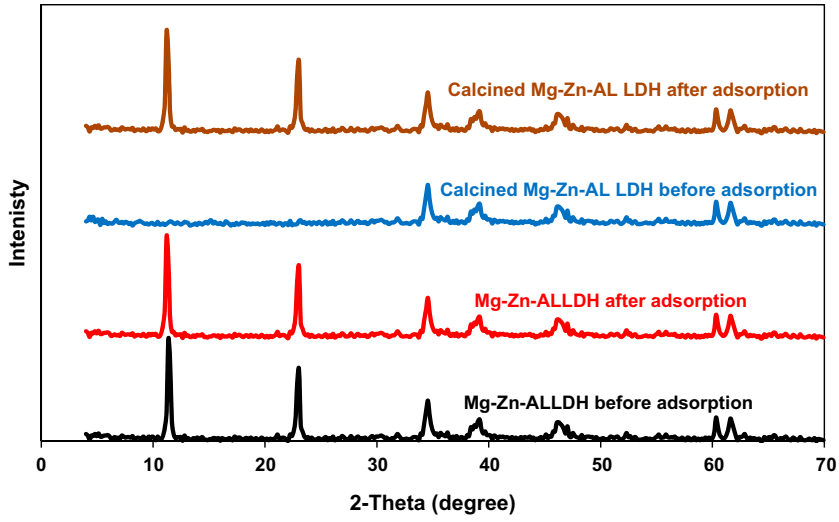

Fig. 1. XRD patterns of the prepared samples.

Table 1
Unit cell parameters and crystal sizes

	Unit cell parameters (Å)		Crystal size (Å)[a]	
Sample	c	a	L_{003}	L_{110}
Mg–Zn–Al LDH	23.4	3.05	47.9	60.4

[a]Calculated using Scherrer's equation, where L is the crystallite Size according to Scherrer's equation.

brucite-like layer and its value depends on the nature of the cations [35]. The unit cell parameter c is related to the thickness of the brucite-like layer and the interlayer distance according to hexagonal stacking. Table 1 presents the crystal sizes, which are calculated using Scherrer's equation.

The real M^{II}/M^{III} molar ratio of Mg–Zn–Al LDH with a chemical composition of $Mg_{0.48}$ $Zn_{0.17}$ $Al_{0.35}$ $(CO_3)_{0.19}{\cdot}H_2O$ was found to be 1.85, where the M^{II}/M^{III} nominal molar ratio was kept constant at 2 during the synthesis.

The Fourier transform infrared spectra of the prepared samples are shown in Fig. 2. The FTIR spectrum of the Mg–Zn–Al LDH clearly showed an O–H stretching vibration of the water molecule in the brucite-like layers at 3,450 cm^{-1}, O–H bending mode in water molecule at 1,640 cm^{-1}, OH stretching mode of interlayer water molecules hydrogen-bonded to interlayer anions at 3,000 cm^{-1}, and CO_3^{2-} anions in the interlayer region at 1,370 cm^{-1} [36–39]. A characteristic band in the low frequency region, corresponding to vibration modes and ascribed to M–O vibration at 1,000 cm^{-1} [40]. The weak shoulder at 788 cm^{-1}can be attributed to Al–O– bond vibrations.

The adsorption–desorption isotherm of the prepared Mg–Zn–Al LDH is shown in Fig. 3a and that of the calcined Mg–Zn–Al LDH is shown in Fig. 3b. They can be classified as type II according to IUPAC classification where no hysteresis is displayed [41]. This type indicates the presence of aggregates (assemblage of particles which are loosely coherent) of plate-like particles giving rise to slit-shaped pores with non-uniform size and shape [42]. The value of average pore radius r that represents half the slit width is calculated as $r = (V_p/A_{BET})$, where V_p is the total pore volume taken at $P/P_o \approx 1.0$, and A_{BET} is the specific surface area obtained using the BET equation taken at $P/P_o = 0.98$ [41,43]. The values listed in Table 2 indicate that the full width of pores of the prepared Mg–Zn–Al LDH and calcined Mg–Zn–Al LDH is 24 and 73.06 Å, respectively, which lies in the initial part of the range of pore sizes that assigned to mesoporosity. The pore size distribution values were determined by the Brunauer–Joyner–Hallenda (BJH) method applied to the desorption branch and t-plot method was used to calculate the type of pores [44]. Thus, the calcined Mg–Zn–Al LDH has higher value of A_{BET}, higher value of V_p, and average pore radius than that of the prepared Mg–Zn–Al LDH. Therefore, the

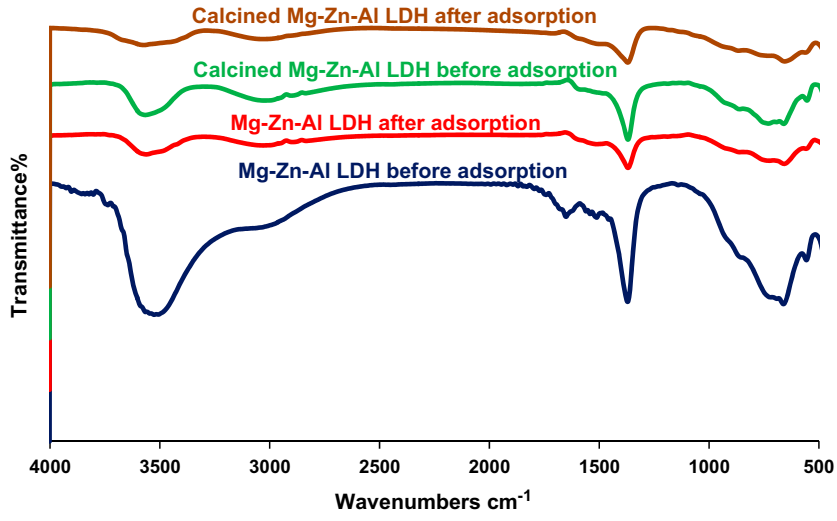

Fig. 2. FTIR spectra of the prepared samples.

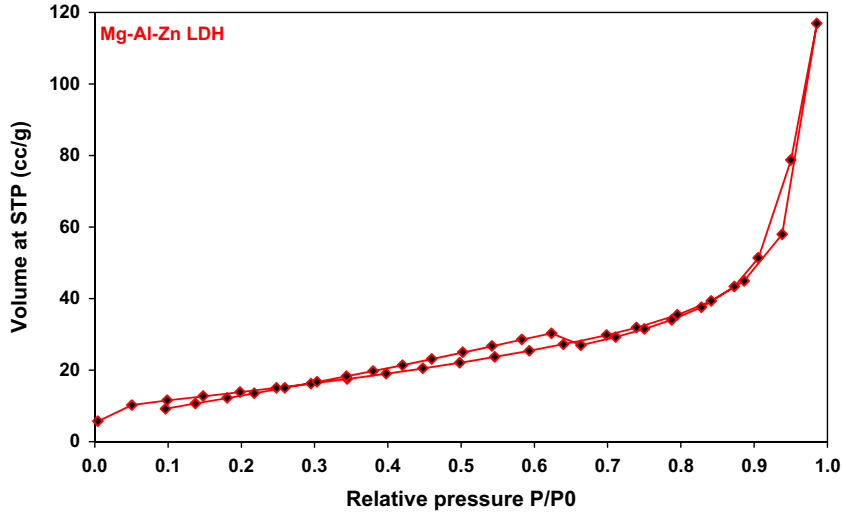

Fig. 3a. N_2 adsorption–desorption isotherm of the prepared Mg–Zn–AL LDH.

higher extent of Cr(VI) adsorption in case of the calcined Mg–Zn–Al LDH can be attributed to the higher surface area, presence of a relatively greater number of narrow mesopores, and total pore volume that are known to furnish a high measurable adsorption capacity than the prepared Mg–Zn–Al LDH. This could be explained as the calcination of Mg–Zn–Al LDH may result in an increase in the interlayer spaces distortion resulting in an increase in the area, total pore volume, and pore radius.

The thermogravimetric analysis of the prepared Mg–Zn–Al LDH is shown in Fig. 4. The first weight loss at lower temperatures (40–180˚C) corresponds to the removal of physically adsorbed water molecules on the surface and interlayer space. The second one, at higher temperatures (180–260˚C), is due to the dehydroxylation of the brucite-like sheets as well as the decomposition of the carbonate anions (partial overlap) [45,46]. A small endothermic peak is observed in the range between 300 and 500˚C that probably corresponds to the conversion of the double layer into MgO lattice. Accordingly, the XRD pattern of the Mg–Zn–Al at 450˚C refers to the MgO phase.

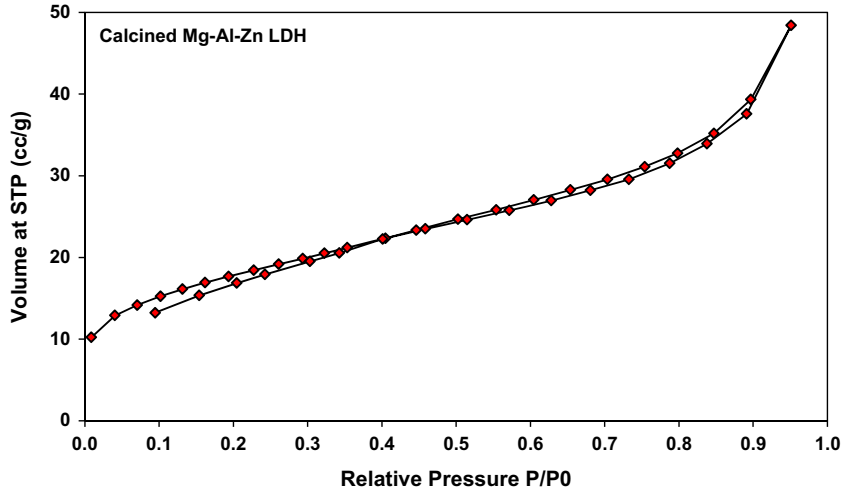

Fig. 3b. N_2 adsorption–desorption isotherm of the calcined Mg–Zn–Al LDH.

Table 2
Surface data of the prepared Mg–Zn–Al LDH and calcined Mg–Zn–Al LDH

Sample	A_{BET} ($m^2\ g^{-1}$)	V_p (mL g^{-1})	$r = V_p/A_{BET}$ (Å)	*C*-value in BET equation
Mg–Zn–Al LDH	51.06	0.07	12	114.86
Calcined Mg–Zn–Al LDH	64.32	0.18	36.53	76.01

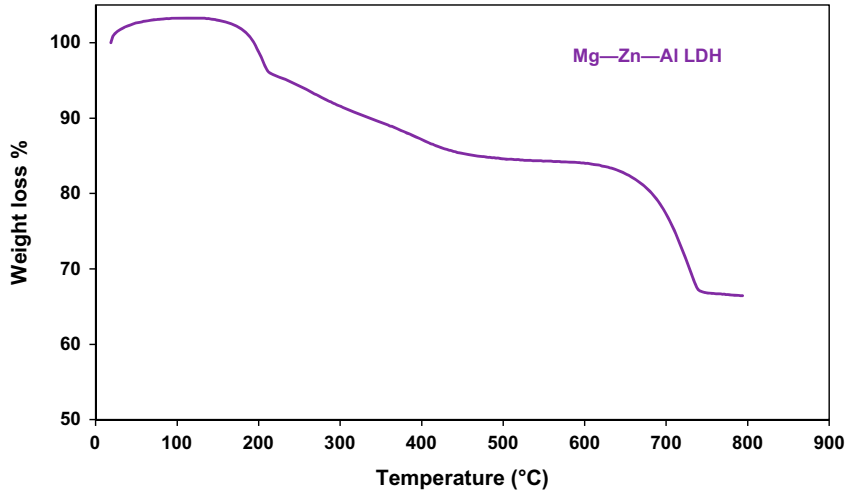

Fig. 4. TGA curve of Mg–Zn–Al LDH.

3.2. *Initial solution pH*

The effect of solution pH on the adsorption capacity and removal percentage of Cr(VI) was investigated, and the results are shown in Fig. 5. The effect of solution pH was tested in the range of 2.0–10 using 0.2 g L^{-1} of adsorbent, Cr(VI) initial concentration of 70 mg L^{-1}, stirring rate of 160 rpm, a contact time of 105 min, and a reaction temperature of 298 K. The results reveal that the amount of Cr(VI) adsorbed on Mg–Zn–Al LDH and calcined Mg–Zn–Al LDH decreases steadily with decreasing pH from 4 to 2, while for pH > 4, the removal seems to be

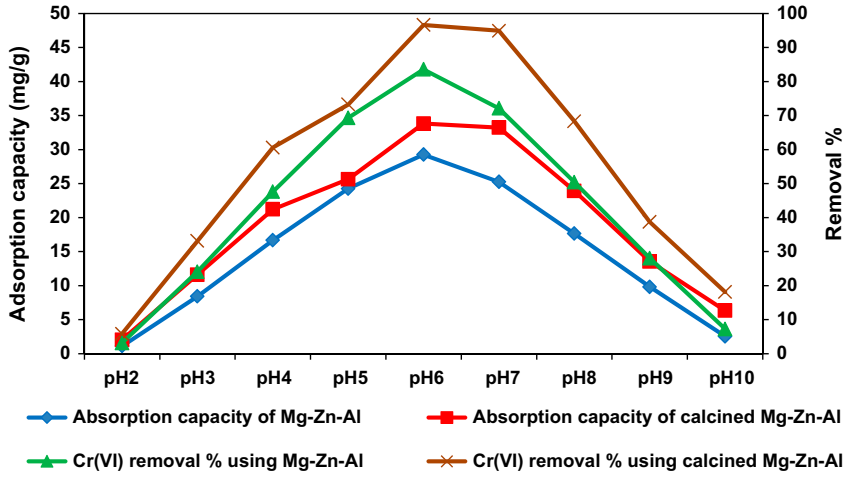

Fig. 5. Effect of initial solution pH on Cr(VI) removal percentage and adsorption capacity using the prepared samples. Reaction conditions: Cr(VI) initial concentration (70 mg L^{-1}), adsorbent mass (0.2 g L^{-1}), stirring rate (160 rpm), 298 K, 105 min.

pH-independent. The decrease in the Cr(VI) removal at lower pH values may be due to the dissolution of LDH at lower pH values [47].

This was confirmed by tracing the soluble species such as Al and Zn in the final solution using the spectrophotometer analysis. While, the decrease in the adsorption percentage at higher pH range may be due to the increase in competitive effect of OH-adsorption on LDH [48]. Fig. 5 shows that above pH 4, the adsorption capacities increase with increasing pH, peaking at pH 6. However, when the pH value exceeds 6, the adsorption capacities decrease slightly. Finally, the adsorption decreased and appeared to reach a plateau in the pH range of ≥5–7. Furthermore, at pH 6 and a reaction temperature of 298 K, the adsorption capacity of Cr(VI) for Mg–Zn–Al LDH and calcined Mg–Zn–Al LDH was 29.25 and 33.82 mg g^{-1}, respectively. While, at pH 10, the adsorption capacity of Cr(VI) for Mg–Zn–Al LDH and calcined Mg–Zn–Al LDH was 2.54 and 6.33 mg g^{-1}, respectively.

3.3. Adsorbent mass

The effect of adsorbent mass on the adsorption capacity and removal percentage of Cr(VI) was investigated, and the results are shown in Fig. 6. The effect of adsorbent mass was tested in the range of 0.1–40 g L^{-1} using Cr(VI) initial concentration of 70 mg L^{-1}, stirring rate of 160 rpm, pH 6, a contact time of 105 min, and a reaction temperature of 298 K. Fig. 6 shows that the Cr(VI) removal percentage increases sharply with increasing the adsorbent mass from 0.1 g L^{-1} to the optimum dose 0.2 g L^{-1}. It reaches 83.56 and 96.63% for Mg–Zn–Al LDH and calcined Mg–Zn–Al LDH, respectively. Complete removal of Cr(VI) was observed at Mg–Zn–Al LDH mass of 0.3 g L^{-1} and at calcined Mg–Zn–Al LDH mass of 0.25 g L^{-1}.

3.4. Equilibrium time

The effect of contact time on the adsorption capacity and removal percentage of Cr(VI) was investigated, and the results are shown in Fig. 7. It is obvious that the adsorption rate of Cr(VI) (70 mg L^{-1}) was considerably fast within the first 30 min, then gradually increased, and finally, the adsorption equilibrium was attained after 105 min using 0.2 g L^{-1} of adsorbent, stirring rate of 160 rpm, pH 6, and a reaction temperature of 298 K.

The initial rapid adsorption may be attributed to the existence of a large number of available sites at the initial stage, and consequently, the increase in adsorbent concentration would increase the Cr(VI) adsorption rate within the initial 30 min. As the time proceeds, the adsorbent concentration is reduced owing to the accumulation of more than 10.83 and 13.75 mg of Cr(VI) adsorbed per gram of adsorbent surface sites after 30 min for Mg–Zn–Al LDH and calcined Mg–Zn–Al LDH, respectively. When the contact time was extended to 105 min, the adsorption capacity was 29.25 and 33.82 mg g^{-1} for Mg–Zn–Al LDH and calcined Mg–Zn–Al LDH, respectively. Lastly, when the contact time was extended to 135 min, the adsorption capacity was 35 mg g^{-1} for both of the adsorbents. The fast Cr(VI) removal rate at the beginning is

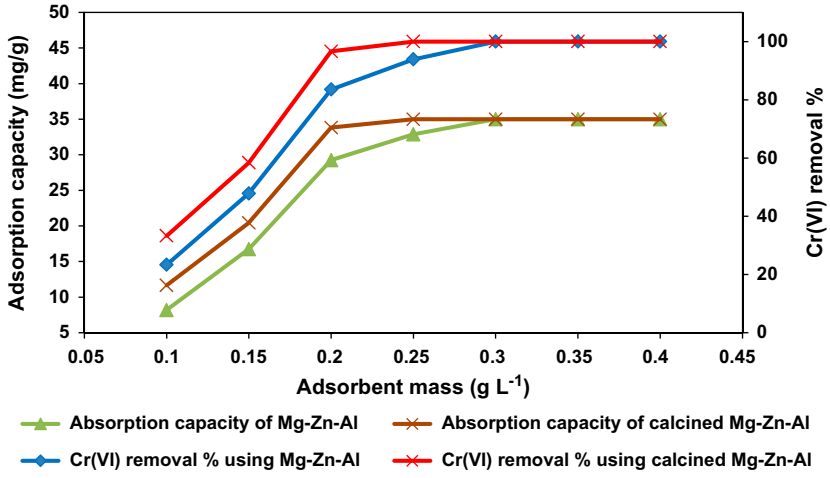

Fig. 6. Effect of adsorbent masses on Cr(VI) removal percentage and adsorption capacity. Reaction conditions: Cr(VI) initial concentration (70 mg L^{-1}), stirring rate (160 rpm), 298 K, pH 6, 105 min.

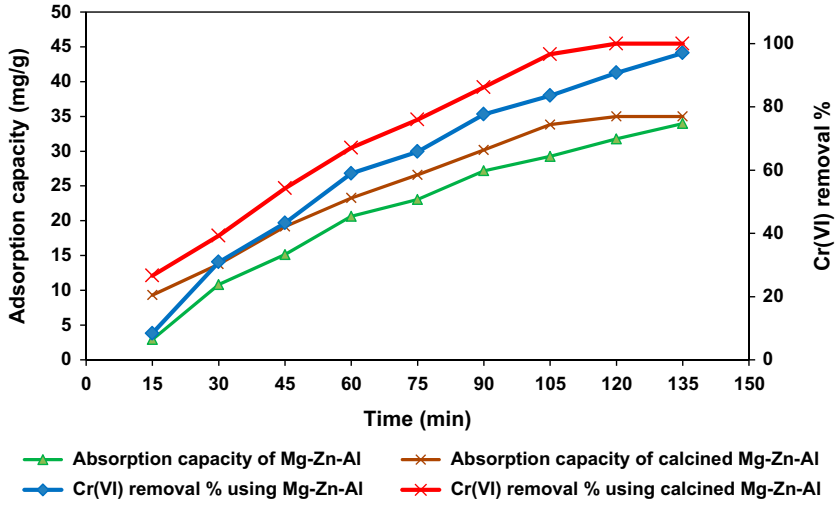

Fig. 7. Effect of contact time on Cr(VI) removal percentage and adsorption capacity using the prepared samples. Reaction conditions: Cr(VI) initial concentration (70 mg L^{-1}), adsorbent mass (0.2 g L^{-1}), stirring rate (160 rpm), 298 K, pH 6.

attributed to the rapid diffusion of Cr(VI) from the solution to the external surfaces of Mg–Zn–Al LDH and also attributed to the longer diffusion range of Cr(VI) into the inner-sphere of Mg–Zn–Al LDH or the ion exchange in the inner surface. Such slow diffusion will lead to a slow increase in the adsorption curve at later stages [49].

3.5. Initial adsorbate concentration

The effect of Cr(VI) initial concentration on the adsorption capacity and removal percentage of Cr(VI) was investigated, and the results are shown in Fig. 8. The effect of Cr(VI) initial concentration was tested in the range of 10–90 mg L^{-1} using 0.2 g L^{-1} of adsorbent, stirring rate of 160 rpm, pH 6, a contact time of 105 min, and a reaction temperature of 298 K. Fig. 8 reveals that the prepared Mg–Zn–Al LDH and calcined Mg–Zn–Al LDH apparently removed a considerable amount of Cr(VI) from the aqueous solutions. The adsorption capacity increased to a certain level, and the active sites became saturated beyond a certain concentration. The decrease in Cr(VI) removal could be explained by the fact that all of the adsorbents had a limited number of active sites, which became saturated above a certain concentration. Fig. 8 also shows

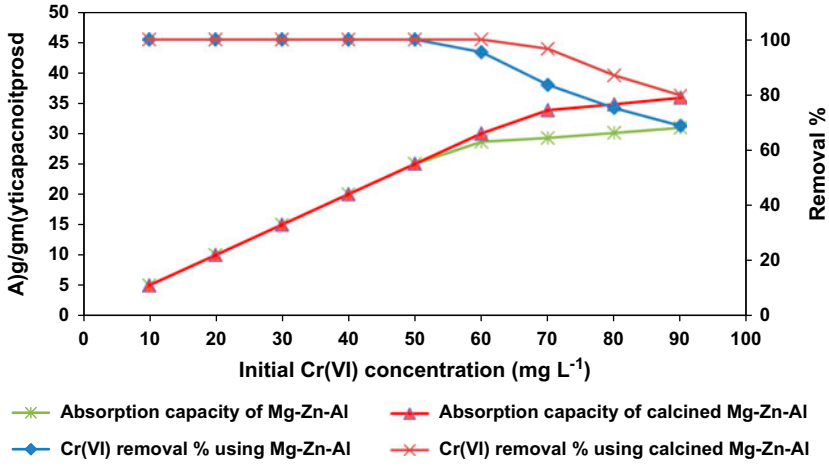

Fig. 8. Effect of initial Cr(VI) concentration on Cr(VI) removal percentage and adsorption capacity using the prepared samples. Reaction conditions: adsorbent mass (0.2 g L^{-1}), stirring rate (160 rpm), 298 K, pH 6, 105 min.

that the maximum efficiency for Cr(VI) adsorption could be obtained over a relatively short period of 105 min. The results reveal that the removal amounts were linearly proportional to the initial metal concentrations. Complete removal of Cr(VI) was observed at initial concentration of 10, 20, 30, 40, and 50 mg L^{-1} for Mg–Zn–Al LDH and at initial concentration of 10, 20, 30, 40, 50, and 60 mg L^{-1} for calcined Mg–Zn–Al LDH. However, when the Cr(VI) initial concentration exceeds 50 mg L^{-1} for Mg–Zn–Al LDH and 60 mg L^{-1} for calcined Mg–Zn–Al LDH, the removal percentages decrease.

Furthermore, the adsorption of Cr(VI) through the rehydration of calcined Mg–Zn–Al LDH is considerably higher than that through the anion exchange of Mg–Zn–Al LDH. A linear increment of adsorption capacity at Cr(VI) concentrations of 10–50 mg L^{-1} for Mg–Zn–Al LDH and of 10–60 mg L^{-1} for calcined Mg–Zn–Al LDH was observed. However, at higher concentrations (more than 50 mg L^{-1} for Mg–Zn–Al LDH and 60 mg L^{-1} for calcined Mg–Zn–Al LDH), a slow increase in the adsorption with increasing the Cr(VI) initial concentration was observed. The latter results are due to the slow anion exchange ability of the Mg–Zn–Al LDH caused by tightly held layers with CO_3^{2-} in the interlayer positions [50,51].

3.6. Adsorption mechanism

Researchers [52,53] have reported that the removal of Cr(VI) resulted from either the anion exchange between interlayer anions of LDHs and Cr(VI) oxyanions or the surface complexation between Cr(VI) oxyanions and inner and outer hydroxyl groups of LDH surfaces as shown in Fig. 9. The surface complexation may occur through the chemical and physical complex between Cr(VI) anions and protonated hydroxyl groups of the LDH surfaces [54]. To check the existence of the intercalation or anion exchange process, the FTIR spectra of Mg–Zn–Al LDH and calcined Mg–Zn–Al LDH before and after Cr(VI) adsorption were determined, as shown in Fig. 2. After adsorption of Cr(VI), the intensity of the characteristic band of CO_3^{2-} anions decreased, indicating that these

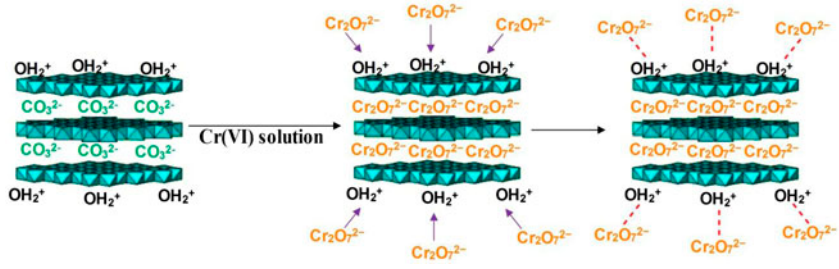

Fig. 9. Schematic of Cr(VI) removal using LDHs.

interlayer anions were replaced by Cr(VI) anions in solution. The main vibration bands for Cr(VI) are located at 940 (Cr–O) and 750 (Cr–O) cm^{-1} [55]. No vibration bands are observed around 750 cm^{-1}. Meanwhile, the band at 940 cm^{-1} could be overlapped with M–O vibrations from the LDH. Therefore, the presence of adsorbed Cr(VI) species cannot be ruled out [56].

4. Conclusion

In this work, Mg–Zn–Al LDH and calcined Mg–Zn–Al LDH were prepared and well characterized using XRD, XRF, FTIR, N_2 adsorption–desorption, and TGA. The obtained solids were tested in the removal of Cr(VI) from aqueous solutions. The adsorption process was optimized in terms of initial solution pH, adsorbent mass, equilibrium time, and initial adsorbate concentration. Maximum adsorption capacity of 29.25 and 33.82 mg g^{-1} for Mg–Zn–Al LDH and calcined Mg–Zn–Al LDH, respectively, was achieved using Cr(VI) initial concentration of 70 mg L^{-1}, 0.2 g L^{-1} of adsorbent, stirring rate of 160 rpm, pH 6, a contact time of 105 min, and a reaction temperature of 298 K. This work opened an opportunity for a low-cost treatment method for Cr(VI) removal from aqueous solutions.

References

[1] R. Ansari, N.K. Fahim, Application of polypyrrole coated on wood sawdust for removal of Cr(VI) ion from aqueous solutions, React. Funct. Polym. 67 (2007) 367–374.

[2] M. Bhaumik, A. Maity, V.V. Srinivasu, M.S. Onyango, Enhanced removal of Cr(VI) from aqueous solution using polypyrrole/Fe_3O_4 magnetic nanocomposite, J. Hazard. Mater. 190 (2011) 381–390.

[3] B. Beverskog, I. Puigdomenech, Revised pourbaix diagrams for chromium at 25–300˚C, Corros. Sci. 39 (1997) 43–57.

[4] B. Saha, C. Orvig, Biosorbents for hexavalent chromium elimination from industrial and municipal effluents, Coord. Chem. Rev. 254 (2010) 2959–2972.

[5] WHO, Guidelines for Drinking-Water Quality, fourth ed., World Health Organization, Geneva, 2011.

[6] A. Baral, R.D. Engelken, Chromium-based regulations and greening in metal finishing industries in the USA, Environ. Sci. Policy 5 (2002) 121–133.

[7] B. Saoudi, N. Jammul, M.L. Abel, M.M. Chehimi, G. Dodin, DNA adsorption onto conducting polypyrrole, Synth. Met. 87 (1997) 97–103.

[8] D.C. Sharma, C.F. Forster, The treatment of chromium wastewaters using the sorptive potential of leaf mould, Bioresour. Technol. 49 (1994) 31–40.

[9] G. Rojas, J. Silva, J.A. Flores, A. Rodriguez, M. Ly, H. Maldonado, Adsorption of chromium onto cross-linked chitosan, Sep. Purif. Technol. 44 (2005) 31–36.

[10] K.Z. Elwakeel, Environmental application of chitosan resins for the treatment of water and wastewater: A review, J. Dispersion Sci. Technol. 31 (2010) 273–288.

[11] V.A. Spinelli, M.C. Laranjeira, V.T. Fávere, Preparation and characterization of quaternary chitosan salt: Adsorption equilibrium of chromium(VI) ion, React. Funct. Polym. 61 (2004) 347–352.

[12] F. Gode, E.D. Atalay, E. Pehlivan, Removal of Cr(VI) from aqueous solutions using modified red pine sawdust, J. Hazard. Mater. 152 (2008) 1201–1207.

[13] L. Monser, N. Adhoum, Modified activated carbon for the removal of copper zinc chromium and cyanide from wastewater, Sep. Purif. Technol. 26 (2002) 137–146.

[14] F. Gode, E. Moral, Column study on the adsorption of Cr(III) and Cr(VI) using Pumice Yarıkkaya brown coal Chelex-100 and Lewatit MP 62, Bioresour. Technol. 99 (2008) 1981–1991.

[15] R.A. Jacques, R. Bernardi, M. Caovila, E.C. Lima, F.A. Pavan, J.C. Vaghetti, C. Airoldi, Removal of Cu(II), Fe(III), and Cr(III) from aqueous solution by aniline grafted silica gel, Sep. Sci. Technol. 42 (2007) 591–609.

[16] F.I. El-Dib, M.H.M. Hussein, H.H.H. Hefni, G. Eshaq, A.E. ElMetwally, Synthesis and characterization of crosslinked chitosan immobilized on bentonite and its grafted products with polyaniline, J. Appl. Polym. Sci. 131 (2014) 41078–41084.

[17] E.M. Seftel, M.C. Puscasu, M. Mertens, P. Cool, G. Carja, Fabrication of CeO_2/LDHs self-assemblies with enhanced photocatalytic performance: A case study on ZnSn-LDH matrix, Appl. Catal. B: Environ. 164 (2015) 251–260.

[18] M. Shao, J. Han, M. Wei, D.G. Evans, X. Duan, The synthesis of hierarchical Zn–Ti layered double hydroxide for efficient visible-light photocatalysis, Chem. Eng. J. 168 (2011) 519–524.

[19] F. Cavani, F. Trifirò, A. Vaccari, Hydrotalcite-type anionic clays: Preparation properties and applications, Catal. Today 11 (1991) 173–301.

[20] V. Rives (Ed.), Layered Double Hydroxides: Present and Future Nova Publishers, New York, 2001.

[21] F. Figueras, Base catalysis in the synthesis of fine chemicals, Top. Catal. 29 (2004) 189–196.

[22] P. Kumbhar, Modified Mg–Al hydrotalcite: A highly active heterogeneous base catalyst for cyanoethylation of alcohols, Chem. Commun. 10 (1998) 1091–1092.

[23] F. Figueras, J. Lopez, J. Sanchez-Valente, T.T.H. Vu, J.M. Clacens, J. Palomeque, Isophorone isomerization as model reaction for the characterization of solid bases: Application to the determination of the number of sites, J. Catal. 211 (2002) 144–149.

[24] K.H. Goh, T.T. Lim, Z. Dong, Application of layered double hydroxides for removal of oxyanions: A review, Water Res. 42 (2008) 1343–1368.

[25] X. Liang, Y. Zang, Y. Xu, X. Tan, W. Hou, L. Wang, Y. Sun, Sorption of metal cations on layered double hydroxides, Colloids Surf., A: Physicochem. Eng. Aspects 433 (2013) 122–131.

[26] A.A. Bakr, M.S. Mostafa, G. Eshaq, M.M. Kamel, Kinetics of uptake of Fe(II) from aqueous solutions by Co/Mo layered double hydroxide (Part 2), Desalin. Water Treat. 56 (2015) 248–255.

[27] M.S. Mostafa, A.A. Bakr, G. Eshaq, M.M. Kamel, Novel Co/Mo layered double hydroxide: Synthesis and uptake of Fe(II) from aqueous solutions (Part 1), Desalin. Water Treat. 56 (2015) 239–247.
[28] N.K. Lazaridis, D.D. Asouhidou, Kinetics of sorptive removal of chromium(VI) from aqueous solutions by calcined Mg–Al–CO_3 hydrotalcite, Water Res. 37 (2003) 2875–2882.
[29] E. Alvarezayuso, H.W. Nugteren, Purification of chromium(VI) finishing wastewaters using calcined and uncalcined Mg–Al–CO-hydrotalcite, Water Res. 39 (2005) 2535–2542.
[30] X.Y. Yu, T. Luo, Y. Jia, R.X. Xu, C. Gao, Y.X. Zhang, J.-H. Liu, X.J. Huang, Three-dimensional hierarchical flower-like Mg–Al-layered double hydroxides: Highly efficient adsorbents for As(V) and Cr(VI) removal, Nanoscale 4 (2012) 3466–3474.
[31] L. Xiao, W. Ma, M. Han, Z. Cheng, The influence of ferric iron in calcined nano-Mg/Al hydrotalcite on adsorption of Cr(VI) from aqueous solution, J. Hazard. Mater. 186 (2011) 690–698.
[32] T. Kameda, E. Kondo, T. Yoshioka, Preparation of Mg–Al layered double hydroxide doped with Fe^{2+} and its application to Cr(VI) removal, Sep. Purif. Technol. 122 (2014) 12–16.
[33] A.A. Bakr, G. Eshaq, A.M. Rabie, A.H. Mady, A.E. ElMetwally, Cupper ions removal from aqueous solutions by novel Ca–Al–Zn layered double hydroxides, Desalin. Water Treat. 1–12 (2015), doi: 10.1080/19443994.2015.1051126.
[34] A. Legrouri, M. Lakraimi, A. Barroug, A. De Roy, J.P. Besse, Removal of the herbicide 2, 4-dichlorophenoxyacetate from water to zinc–aluminium–chloride layered double hydroxides, Water Res. 39 (2005) 3441–3448.
[35] R.R. Delgado, C.P. De Pauli, C.B. Carrasco, M.J. Avena, Influence of M^{II}/M^{III} ratio in surface-charging behavior of Zn–Al layered double hydroxides, Appl. Clay Sci. 40 (2008) 27–37.
[36] V. Rives, S. Kannan, Layered double hydroxides with the hydrotalcite-type structure containing Cu^{2+}, Ni^{2+}, and Al^{3+}, J. Mater. Chem. 10 (2000) 489–495.
[37] W. Yang, Y. Kim, P.K. Liu, M. Sahimi, T.T. Tsotsis, A study by in situ techniques of the thermal evolution of the structure of a Mg–Al–CO_3 layered double hydroxide, Chem. Eng. Sci. 57 (2002) 2945–2953.
[38] Y.M. Zheng, N. Li, W.D. Zhang, Preparation of nanostructured microspheres of Zn–Mg–Al layered double hydroxides with high adsorption property, Colloids Surf., A: Physicochem. Eng. Aspects 415 (2012) 195–201.
[39] T. Hibino, Y. Yamashita, K. Kosuge, A. Tsunashima, Decarbonation behavior of Mg–Al–CO_3 hydrotalcite-like compounds during heat treatment, Clays Clay Miner. 43 (1995) 427–432.
[40] M. Lakraimi, A. Legrouri, A. Barroug, A. De-Roy, J.P. Besse, Preparation of a new stable hybrid material by chloride–2 4-dichlorophenoxyacetate ion exchange into the zinc–aluminium–chloride layered double hydroxide, J. Mater. Chem. 10 (2000) 1007–1011.
[41] K.S. Sing, Reporting physisorption data for gas/solid systems with special reference to the determination of surface area and porosity, Pure Appl. Chem. 57 (1985) 603–619.
[42] A. Lecloux, J.P. Pirard, The importance of standard isotherms in the analysis of adsorption isotherms for determining the porous texture of solids, J. Colloid Interface Sci. 70 (1979) 265–281.
[43] S. Brunauer, P.H. Emmett, E. Teller, Adsorption of gases in multimolecular layers, J. Am. Chem. Soc. 60 (1938) 309–319.
[44] E.P. Barrett, L.G. Joyner, P.P. Halenda, The determination of pore volume and area distributions in porous substances. I. Computations from nitrogen isotherms, J. Am. Chem. Soc. 73 (1951) 373–380.
[45] R.L. Frost, W. Martens, Z. Ding, J.T. Kloprogge, DSC and high-resolution TG of synthesized hydrotalcites of Mg and Zn, J. Therm. Anal. Calorim. 71 (2003) 429–438.
[46] R.L. Frost, W.N. Martens, K.L. Erickson, Thermal decomposition of the hydrotalcite, J. Therm. Anal. Calorim. 82 (2005) 603–608.
[47] M.C. Hermosín, I. Pavlovic, M.A. Ulibarri, J. Cornejo, Hydrotalcite as sorbent for trinitrophenol: Sorption capacity and mechanism, Water Res. 30 (1996) 171–177.
[48] L. Yang, Z. Shahrivari, P.K. Liu, M. Sahimi, T.T. Tsotsis, Removal of trace levels of arsenic and selenium from aqueous solutions by calcined and uncalcined layered double hydroxides (LDH), Ind. Eng. Chem. Res. 44 (2005) 6804–6815.
[49] M.H. Al-Qunaibit, W.K. Mekhemer, A.A. Zaghloul, The adsorption of Cu(II) ions on bentonite—A kinetic study, J. Colloid Interface Sci. 283 (2005) 316–321.
[50] S. Miyata, Physico-chemical properties of synthetic hydrotalcites in relation to composition, Clays Clay Miner. 28 (1980) 50–56.
[51] C.S. Wang, K.B. Benkendorfer, J.L. Burba III, Halide removal from fluid organic materials. US Patent No 4511710, 1985.
[52] Y. Li, B. Gao, T. Wu, D. Sun, X. Li, B. Wang, F. Lu, Hexavalent chromium removal from aqueous solution by adsorption on aluminum magnesium mixed hydroxide, Water Res. 43 (2009) 3067–3075.
[53] R.L. Goswamee, P. Sengupta, K.G. Bhattacharyya, D.K. Dutta, Adsorption of Cr(VI) in layered double hydroxides, Appl. Clay Sci. 13 (1998) 21–34.
[54] F. Zhang, N. Du, H. Li, X. Liang, W. Hou, Sorption of Cr(VI) on Mg–Al–Fe layered double hydroxides synthesized by a mechanochemical method, RSC Adv. 4 (2014) 46823–46830.
[55] Y.G. Ko, U.S. Choi, T.Y. Kim, D.J. Ahn, Y.J. Chun, FT-IR and isotherm study on anion adsorption onto novel chelating fibers, Macromol. Rapid Commun. 23 (2002) 535–539.
[56] C. Alanis, R. Natividad, C. Barrera-Diaz, V. Martínez-Miranda, J. Prince, J.S. Valente, Photocatalytically enhanced Cr(VI) removal by mixed oxides derived from MeAl (Me: Mg and/or Zn) layered double hydroxides, Appl. Catal. B: Environ. 140–141 (2013) 546–551.